This article has been accepted for publication in a future issue of this journal, but has not been fully edited. Content may change prior to final publication. Citation information: DOI 10.1109/TIA.2018.2793213, IEEE Transactions on Industry Applications



# Design and Control of Micro-Grid fed by Renewable Energy Generating Sources

Shailendra Kr. Tiwari[*], *Member, IEEE,* Bhim Singh[*], *Fellow, IEEE,* Puneet K. Goel[$]
[*] Department of Electrical Engineering, IIT Delhi, New Delhi, India
[$] South MCD, Dr. SPM Civic Centre, New Delhi, India

***Abstract*— This paper presents a control of a micro-grid at an isolated location fed from wind and solar based hybrid energy sources. The machine used for wind energy conversion is doubly fed induction generator (DFIG) and a battery bank is connected to a common DC bus of them. A solar photovoltaic (PV) array is used to convert solar power, which is evacuated at the common DC bus of DFIG using a DC-DC boost converter in a cost effective way. The voltage and frequency are controlled through an indirect vector control of the line side converter, which is incorporated with droop characteristics. It alters the frequency set point based on the energy level of the battery, which slows down over charging or discharging of the battery. The system is also able to work when wind power source is unavailable. Both wind and solar energy blocks, have maximum power point tracking (MPPT) in their control algorithm. The system is designed for complete automatic operation taking consideration of all the practical conditions. The system is also provided with a provision of external power support for the battery charging without any additional requirement. A simulation model of system is developed in Matlab environment and simulation results are presented for various conditions e.g. unviability of wind or solar energies, unbalanced and nonlinear loads, low state of charge of the battery. Finally a prototype of the system is implemented using a 5 kW solar PV array simulator and a 3.7 kW wound rotor induction machine and experimental results are produced to reaffirm the theoretical model and design.**

***Keywords*— *DFIG, Vector Control, Wind Energy; Power Quality, Solar PV Energy, Micro-grid, Battery Energy Storage System, Renewable Energy System.***

## I. INTRODUCTION

There are many remote locations in the world, which don't have access to electricity. There are also many places, which are connected to the grid, however, they don't receive electricity for up to 10-12 hours in the day and as a result of it, economic activities of inhabitants suffer. Many of such places are rich in renewable energy (RE) sources such as wind, solar and bio-mass. An autonomous generation system utilising locally available RE sources, can greatly reduce the dependency on the grid power, which is predominantly fossil power. Wind and solar energy sources, are more favorite than bio-mass based system as latter is susceptible to supply chain issue. However, wind and solar energies suffer from high level of power variability, low capacity utilization factor combined with unpredictable nature. As a result of these factors, firm power cannot be guaranteed for autonomous system. While the battery energy storage (BES) can be helpful of lowering power fluctuation and increasing predictability, utilisation factor can be increased by operating each energy source at optimum operating point. The optimum operating point also called as maximum power point tracking (MPPT), requires regulation of the operating point of wind energy generator and solar PV (Photovoltaic) array in term of speed and voltage to extract maximum electrical energy from input resource. The MPPT can be achieved by power electronics (PE) based control. PE based control can also help energy management for BES.

Many authors have reported autonomous solar PV systems [1-2] and autonomous wind energy systems [3-4]. However, autonomous system with only one source of energy, requires very large size of storage and associated PE components.

A hybrid energy system consisting of two or more type of energy sources, has ability to reduce the BES requirement and increases reliability. Wind and solar energies are natural allies for hybridization. Both have been known to be complementary to each other in daily as well as yearly pattern of the behavior. Acknowledging advantages of this combination, many authors have presented autonomous wind solar hybrid systems [5-10]. The most favorite machine for small wind power application, is permanent magnet synchronous generator [4-5]. It is possible to achieve gearless configuration with PMSG, however, it requires 100% rated converter in addition to costlier machine [11]. Some authors have also used wind solar hybrid system with a squirrel cage induction generator (SCIG) [6], Though SCIG has commercial edge regarding machine cost, however, the scheme doesn't have speed regulation required to achieve MPPT. Moreover, if the speed regulation is done, it requires full power rated converter.

A doubly fed induction generator (DFIG) as a generator is commonly used for commercial wind power generation and its applications, have been presented by many authors in their publications for autonomous application along with solar PV array [7-10]. DFIG may operate variable speed operation with lower power rated converters. However, to work the system as a micro-grid, the generated voltage should be balanced and THD (Total Harmonics Distortion), must be within requirement of IEEE-519 standard at no-load, unbalanced load as well as nonlinear load. Moreover, both the wind and solar energies sources should operate at MPPT. None of the authors, has reported all these issues. They have not presented performance parameters e.g. power quality, system efficiency etc under the different operating conditions. Moreover, they also lack experimental verification.

This paper presents a micro-grid fed from wind and solar based renewable energy generating sources (REGS). DFIG is used for wind power conversion while crystalline solar photovoltaic (PV) panels are used to convert solar energy. The control of overall scheme, helps to provide quality power to its consumers for all conditions e.g. no-load, nonlinear load and unbalanced loads. The controls of both generating sources, are equipped with MPPT. Emmanouil *et al.* [12] have proposed a droop based control system for micro-grid with the help of standalone battery converter. In the presented scheme, the droop characteristic is embedded in control of load side converter (LSC) of DFIG. This function varies the system

This article has been accepted for publication in a future issue of this journal, but has not been fully edited. Content may change prior to final publication. Citation information: DOI 10.1109/TIA.2018.2793213, IEEE Transactions on Industry Applications



frequency based on state of charge of the battery and slows down deep discharge and over-charge of the battery.

The DFIG in a proposed system, has also two voltage source converters (VSC). In addition to LSC, DFIG also has another VSC connected to rotor circuit termed as rotor side converter (RSC). The function of RSC is to achieve wind MPPT (W-MPPT). The solar PV system is connected to the DC bus through solar converter, which boosts the solar PV array voltage. With this configuration, the solar power can be evacuated in a cost effective way. This converter too is equipped with solar MPPT(S-MPPT) control strategy to extract maximum solar energy. In case of unavailabity of wind energy source and lower state of charge of the battery, the battery bank can be charged through the grid power or a diesel generator through the same RSC. With the help of the LSC, rated frequency and voltage at the load terminals, are maintained under following conditions.

- Varying amount of solar and wind powers.
- Unavailability of solar power or wind power.
- Loss of load or breakdown of the distribution system.
- Different types of loads as unbalanced and nonlinear loads.

It presents the design criteria of major components and control strategies for various converters. Finally it presents simulation results followed by experimental results obtained on a prototype developed in the laboratory.

## II. SYSTEM COMPONENTS DESCRIPTION

A single line diagram of the proposed renewable energy generation system (REGS) fed micro-grid is shown in Fig. 1. The same has been designed for location having maximum power demand and average power demand of 15 kW and 5 kW, respectively. The rated capacity of both wind and solar energy block in REGS, is taken as 15 kW. The capacity utilisation factor of 20% is considered for both energy blocks, which is enough to provide full day energy requirement of the hamlet.

As shown in a schematic diagram, the wind energy source is isolated using a 3-pole breaker from the network in case of insufficient wind speed. The DC side of both RSC and LSC along with HV side of solar converter, is connected at the battery bank. RSC helps the wind energy system to run at the optimum rotation speed as required by W-MPPT algorithm. The LSC controls the network voltage and frequency. The energy flow diagram of the system is shown in Fig. 2.

The design methodology of major components of REGS, is shown in following sub-sections.

### *A. Wind Turbine and Gear*

The wind turbine captures the kinetic energy of the wind and provides driving torque for DFIG. The value of captured mechanical power is given as,

$$P_m = 0.5 c_p \pi r^2 \rho V_w^3 \tag{1}$$

Here $V_w$, and $r$, are wind speed and radius of wind turbine respectively. $C_p$ is the coefficient of performance of wind turbine and is mathematically derived as [13],

$$c_p(\lambda,\beta) = 0.73\left(\frac{151}{\lambda_i} - 0.002*\beta^{2.14} - 13.2\right)e^{-(18.4/\lambda_i)} \tag{2}$$

where,

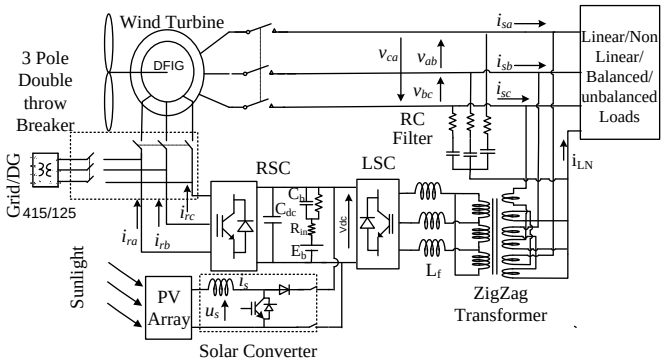


Fig. 1 Schematic of isolated micro-grid network fed by renewable energy source using battery storage

$$\frac{1}{\lambda_i} = \frac{1}{(\lambda + 0.08\beta)} - \frac{0.035}{\beta^3 + 1} \tag{3}$$

$\lambda$ and $\beta$ are the tip speed ratio(TSR) and the turbine blade pitch angle, respectively.

TSR is related to the of the turbine speed $\omega_r$, turbine radius $r$ and wind speed $V_w$ as,

$$\lambda = \omega_r r / (\eta_G V_W) \tag{4}$$

$$\eta_G = \omega_{rm} r / (\lambda^* V_{Wr}) \tag{5}$$

where $\eta_G$ is the turbine shaft gear ratio.

The rated capacity of wind generator used in proposed scheme is 15 kW at a rated wind speed ($V_{wr}$) of 9 m/s and rotational speed ($\omega_{rm}$) of 198 rad/s. The optimum TSR ($\lambda^*$) and turbine radius, are taken 5.67 and 4.3 m, respectively. The control action maintains W-MPPT till the machine speed reaches $\omega_{rm}$. Having known $\lambda^*$, $V_{wr}$ and $\omega_{rm}$, gear ratio $\eta_G$ is determined from (5) as,

$$\eta_G = (198 \times 4.3)/(5.67 \times 9) = 16.68$$

### *B. DFIG*

An external power flow in DFIG, is through both stator and rotor. Neglecting losses, at maximum wind speed, the nominal power of DFIG ($P_e$) is related to rated air gap power ($P_{ag}$) as,

$$P_e = P_{ag}/(1+|s_{pmax}|)) \tag{6}$$

$S_{pmax}$ is the slip corresponding to the turbine speed, $\omega_{rm}$ and its value is -0.267. The speed range of DFIG is the speed corresponding to slip 0.3 to -0.267. Assuming air gap power($P_{ag}$) equal to mechanical input power, the electrical power rating of the machine $P_e$ corresponding to maximum input power, is {15/(1+0.267)} =11.83 kW. When the wind turbine is in service, the complete magnetising power requirement of machine is provided by RSC. Hence 11.83 kW capacity of DFIG is adequate to convert mechanical power from 15 kW wind energy system to electrical energy. Taking additional margin due to electrical losses, a 12.5 kW machine is chosen, which detailed parameters, are given in Appendix A.

### *C. Transformer*

The load and stator terminals are connected to the LSC through a zig-zag transformer, which also provides neutral for single phase loads at 415 V side. The maximum absolute value of rotor slip, is 0.3 and accordingly, the maximum rotor voltage $V_{rmax}$ becomes 125 V(0.3×415 V). The voltage at the LV side of zig-zag transformer is also chosen to be equal to $V_{rmax}$ Accordingly the transformer has a voltage ratio 415/125

This article has been accepted for publication in a future issue of this journal, but has not been fully edited. Content may change prior to final publication. Citation information: DOI 10.1109/TIA.2018.2793213, IEEE Transactions on Industry Applications



V and its HV windings are connected to the stator and the load.

The zig-zag transformer should meet the combined kVA requirement of load as well as connected filters. Accordingly, a 20 kVA transformer is chosen, which is sufficient to transfer rated power along with meeting reactive power requirement of the connected loads and filters at peak demand.

### *D. Battery Sizing*

The maximum operating slip of machine is 0.3. The DFIG speed corresponding to this slip is 110 rad/s. At this slip, the line voltage of rotor $V_{rmax}$ become 125 V (415×0.3). The required DC bus voltage ($V_{dc}$) for PWM control is as,

$$V_{dc} > \{2\sqrt{(2/3)}V_L\}m_i \quad (7)$$

$V_L$ is the higher of the line voltage of low voltage (LV) side of the zig-zag transformer and the rotor voltage at highest slip. The maximum operating slip is 0.3 and accordingly the highest rotor voltage as well as LV side of zig-zag transformer is 125 V. The modulation index, $m_i$ is chosen to be unity. Based on these inputs, the DC bus voltage $V_{dc}$ required for functioning of PWM control must not be less than 204 V. In the presented scheme, $V_{dc}$ is taken 240 V.

The proposed micro-grid is designed to provide load requirement of 5 kW without any generating source for an up to 12 hours. Taking additional 20% margin for energy losses during exchange of energy, the required battery storage capacity becomes 72 kWhr. At the DC bus voltage of 240 V, the Ampere-Hour (AH) rating of battery becomes 300 AH (72,000/240). This is achieved using 40 numbers of 12V, 150 AH lead acid batteries divided equally into two parallel circuits.

A lead acid battery bank can be safely operated between 2.25 V and 1.8 V per cell. This makes the maximum battery voltage $V_{bmax}$ and minimum battery voltage $V_{bmin}$ to be 270 V and 216 V, respectively. A battery bank can be assumed to a DC source with fictitious capacitor $C_b$, internal resistance $R_{in}$ connected in series. In addition to it, another resistance $R_b$ is connected across the battery to denote energy drain due to self discharge of battery.

$C_b$ in series with the battery denotes voltage change due to charging and discharging. The value of $C_b$ is determined as [14],

$$C_b = kWh \times 3600 \times 1000/\{0.5 \times (V_{bmax}^2 - V_{bmin}^2)\} \quad (8)$$

Substituting variables in (8), $C_b$ is obtained 19753 F.

### *E. Solar PV System*

The basic element of a solar PV system is the solar cell, which is based on the work of Rey-Boué et al [15]. The solar panels are configured such that the open circuit voltage of the solar string remains less than the lowest downstream voltage of solar converter or DC bus voltage, $V_{dc}$. The cell numbers ($N_c$) in a string, is a function of its DC voltage and cell open circuit voltage $V_{occ}$ as,

$$N_c = V_{dcm}/V_{occ} \quad (9)$$

The value of $V_{occ}$ based on a typical commercially available cell characteristics and its value, is taken as 0.64 V. As evaluated in sub-section (D), the minimum battery voltage can fall down upto 216 V. Solar array voltage ($u_s$) can vary up to 3%, which is due to manufacturing tolerance of electrical quantities of module. Hence $V_{dcm}$ is taken as 210 V and accordingly, the required numbers of cell, $N_c$ as derived from (9) comes to be 328 cells. To evenly distribute the cells in a standard configuration, 324 cells are taken, which are divided in 9 modules of 36 cells each. The ratio of $V_{occ}$ to cell voltage at maximum power point (MPP), $V_{mpc}$ for a typical module characteristic is 1.223. Accordingly, the module voltage at MPP becomes ($V_{mpc}$ x 36) 18.83 V and $u_s$ becomes 169.47 V.

At 15 kW solar array capacity, the cumulative string current at MPP becomes {15000/(9*18.83)}88.5 A. The number of string in the solar array is chosen to be 11, accordingly module current at MPP, $I_{mp}$ becomes 8.04 A. The ratio of short circuit current $I_{sc}$ to $I_{mp}$ for a typical module is 1.081 and accordingly $I_{sc}$ is taken as 8.69 A.

The detailed parameters used for modeling of solar energy block, are given in Table-I.

### *F. High Pass Filter*

To reduce voltage ripples, a high pass filter is used at stator terminal, which time constant should be less than fundamental frequency i.e. 20 ms. Moreover, it should be tuned half the switching frequency. The switching frequency is 10 kHz and accordingly the filter to be designed for 5 kHz. In the present scheme, a series RC filter consisting of 5 Ω resistance and 15 μF capacitance, is connected at the stator terminals of DFIG. The filter provides less than 5.43 Ω impedance for harmonic voltage having more than 5 kHz frequency.

## III. CONTROL ALGORITHM

As shown in Fig.1, REGS consists of three converters, which control descriptions, are given as follows.

### *A. Control of Solar Converter*

A solar converter, which is a boost type DC-DC converter used to evacuate solar power with embedded S- MPPT logic. It is based on incremental conductance method [16]. The S-MPPT through intelligent switching regulates $u_s$ so as the solar system operates at MPP. The flow diagram of the MPPT algorithm is shown in Fig.3.

### *B. Control of LSC*

Since the onshore wind turbine generates power only for 60-70% of the time, the system should be designed to work when no wind power is available. As shown in the control diagram in Fig. 4, $i^*_{qs}$ consists of two components. The first component, $i_{qs1}$ corresponds to the power component of DFIG current, when wind turbine is in operation. The second components $i_{qs2}$ corresponds to the power component drawn when stator of DFIG is not connected to the load terminal.

TABLE I
TECHNICAL DETAILS OF SOLAR BLOCK

| | |
|---|---|
| Open Circuit Voltage of PV cell, $V_{occ}$ | 0.64 V |
| Open circuit voltage of a module ($V_{oc}$) | 23.04 V |
| MPP voltage of PV cell, $V_{mpc}$ | 0.5223 V |
| MPP Voltage of module($V_{mp}$) | 18.83 V |
| Short Circuit current of module($I_{sc}$) | 8.69 A |
| MPP current of module ($I_{mp}$) | 8.04 A |
| Module Power Rating | 151 Wp |
| $\mu_{Isc}$ | 0.04 %/ °C |
| $\mu_{Voc}$ | -0.36%/ °C |
| PV Modules in the solar block | 11 strings each having 9 PV modules. |
| String open circuit voltage, $u_{soc}$ | 207.36 V |
| Capacity of Solar PV System | 15 kWp |

The direct component of current, $i^*_{ds}$ corresponds to the reactive power requirement at the point of common

This article has been accepted for publication in a future issue of this journal, but has not been fully edited. Content may change prior to final publication. Citation information: DOI 10.1109/TIA.2018.2793213, IEEE Transactions on Industry Applications



interconnection of the generator and filter. The information of $i^*_{qs}$ and $i^*_{ds}$ provides the reference stator currents and help in maintaining the voltage and frequency through the indirect vector control as elaborated in following sub-sections.

*1) Frequency Set point $f^*_s$ Computation:* The stator frequency is controlled by the LSC. Though the system has to generate rated frequency, a droop characteristic has been incorporated which gives frequency set point as,

$$\omega^*_e = 2\times\pi\times[50+\{2\times (V_{dc}\text{-}240)/(V_{dcmax}-V_{dcmin})\}] \quad (10)$$

where $V_{dcmin}$,$V_{dcmax}$ and $V_{dc}$ are the minimum, maximum and instantaneous DC bus voltage, respectively. $V_{dcmax}$ is taken as 272.5 V, which is the bus voltage corresponding $V_{bmax}$ during charging. Similarly, $V_{dcmin}$ is being taken as 213.5 V, which bus voltage corresponds $V_{bmin}$ and the battery being discharged. With these figures, the frequency varies from 49 Hz to 51 Hz.

*2) $i^*_{ds}$ Computation:* $i^*_{ds}$ is the magnetizing component of stator current required at load terminal and is computed as,

$$i^*_{ds(k)} = i_{ds(k-1)} + K_{pv}(v_{err(k)}\text{-}v_{err(k-1)}) + K_{iv}v_{err(k)}\,dt \quad (11)$$

where $V_{err(k)}$ is the voltage error

$$v_{err(k)} = V^*_{Lm} - V_{Lm(k)} \quad (12)$$

$V_{Lm}$ is amplitude of the sensed three phase line voltage at generator terminls on per unit line basis which is derived from the sesned line voltages ($v_{Lab}$, $v_{Lbc}$ and $v_{Lca}$) as,

$$V_{Lm} = \{2(v^2_{Lab}+v^2_{Lbc}+v^2_{Lca})/3\}^{1/2} \quad (13)$$

$V^*_{Lm}$ is reference line voltage, which is kept 585 V.

*3) $i^*_{qs}$ Computation:* As discussed, $i^*_{qs}$ is divided into two sub-components as,

$$i^*_{qs} = i^*_{qs1} + i^*_{qs2} \quad (14)$$

$i^*_{qs1}$ is the quadrature component of the generator along the stator field and is computed as,

$$i^*_{qs1(k)} = -L_m * i_{qr(k)} / L_s \quad (15)$$

$i^*_{qs2}$ is the required quadrature of stator current when DFIG is not connected to the LSC(or load) on account of low wind speed or fault. It is the evaluated as follows,

$$i^*_{qs2(k)} = i_{qs2(k-1)} + K_{p\omega e}(\omega_{eerr(k)}\text{-}\omega_{eerr(k-1)}) + K_{i\omega e}\omega_{eerr(k)}\,dt \quad (16)$$

$\omega_{eerr}$ is the error of rated frequency $\omega^*_e$ as computed from (10) and actual frequency $\omega_e$. The evaluated values of DC quantities $i^*_{ds}$ and $i^*_{qs}$ are transformed to AC quantities $i^*_{sa}$, $i^*_{sb}$ and $i^*_{sc}$ using angle $\theta_{statorflux}$ which is derived as,

$$\theta_{statorflux} = \int_0^t \omega^*_e dt \quad (17)$$

$i_{ds}$ and $i_{qs}$ are transformed to 3-phase quantities using transformation angle $\theta_{statorflux}$. The derived 3-phase quantities and the sensed stator currents in a hysteresis current regulator give switching pulses to the converters.

### C. Control of RSC

RSC regulates the speed of turbine so that the system operates at MPP irrespective of varying wind conditions. It also provides magnetizing power to the generator. The control philosophy as shown in Fig. 5, includes control algorithm for determination of quadrature and direct components of rotor currents, $I_{qr}$, $I_{dr}$ and transformation angle, $\theta_{slip}$.

*1) $i^*_{dr}$ Computation:* $i_{dr}$ is related to magnetizing power of machine in field oriented vector control(FOVC). The no-load magnetizing power is to be supplied through RSC and the corresponding $i_{dr}$ is as,

$$i^*_{dr} = I_{ms0} = V^*_{Lm}/(\sqrt{3}X) \quad (18)$$

where, $X_m$ is magnetizing reactance of the DFIG. $V^*_{Lm}$ is the reference amplitude of line voltage as derived from (13).

*2) $i^*_{qr}$ Computation:* In FOVC at constant stator flux $\phi_{ds}$, the quadrature component of the rotor current, $i^*_{qr}$ is proportional to the torque [17].

$i^*_{qr}$ is derived from output of the PI speed controller as,

$$i^*_{qr(k)} = i_{qr(k-1)} + K_{p\omega r}(\omega_{rerr(k)}\text{-}\omega_{err(k-1)}) + K_{i\omega r}\omega_{rerr(k)}\,dt \quad (19)$$

$K_{pr}$ and $K_{ir}$ are proportional and integral gains of PI speed controller.

$\omega_{rerr(k)}$ is speed error between reference and sensed speed as,

$$\omega_{rerr(k-1)} = \omega_{r(k)}\text{-}\omega^*_{r(k)} \quad (20)$$

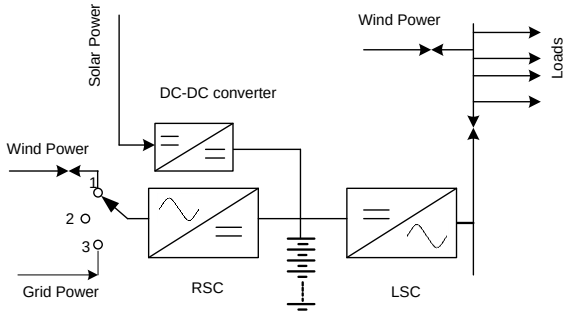


Fig. 2 Energy flow diagram of isolated micro-grid network fed by renewable energy source using battery storage

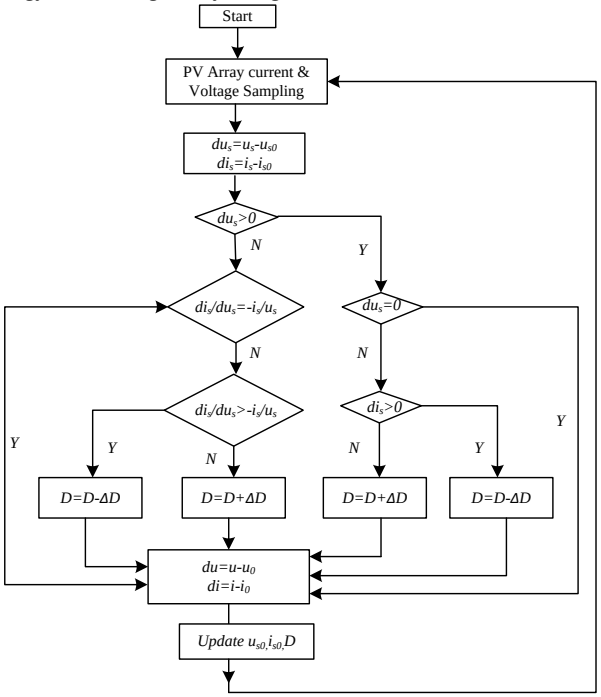


Fig. 3 Flow-diagram of solar MPPT algorithm

This article has been accepted for publication in a future issue of this journal, but has not been fully edited. Content may change prior to final publication. Citation information: DOI 10.1109/TIA.2018.2793213, IEEE Transactions on Industry Applications



$\omega^*_r$ is reference generator speed which is derived from (5) as,

$$\omega^*_r = k \times \eta_G \times V_W / r \quad (21)$$

Here *'k'* is constant factor, which alters the wind speed setpoint to deviate from MPP and can help to check voltage rise in case of low load demand and high generation. The value of *k* is determined from the two relays namely, $k_1$ and $k_2$ as shown in Fig. 5. The output of relay falls to 0.85 if the DC bus voltage increases beyond threshold value. The threshold values of both relay, are kept 260 and 265, respectively. The *k* attains values of 0.85 and 0.72 as the $V_{dc}$ exceeds 260 V and 265 V, respectively.

The evaluated values of $i_{dr}^*$ and $i_{qr}^*$ are transformed to AC reference rotor currents $i_{ra}^*$, $i_{rb}^*$ and $i_{rc}^*$ using transformation angle $\theta_{slip}$. $\theta_{slip}$ is determined as,

$$\theta_{slip} = \int_0^t (\omega^*_e - (p/2)\omega_r)dt \quad (22)$$

The error signals of reference currents and sensed currents ($i_{ra}$, $i_{rb}$ and $i_{rc}$) through hysteresis current regulator, generate control signals for RSC.

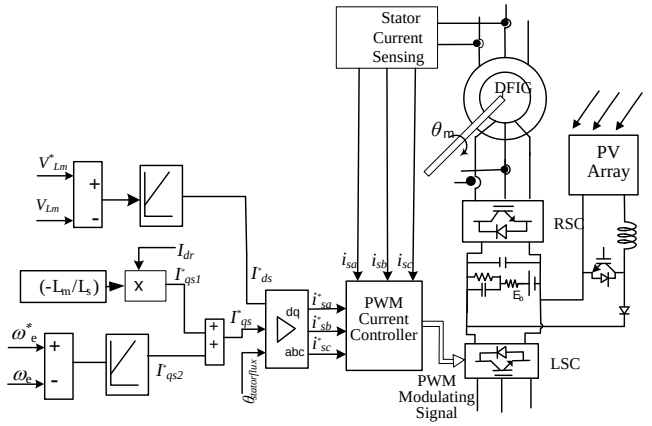


Fig. 4 Control diagram of LSC for REGS energy fed micro-grid

*3) Battery Charging Mode:* The battery charging mode, is selected as per control diagram shown in Fig. 6. The battery charging is achieved by direct vector control of rotor current.

The direct component of the rotor current along voltage axis, corresponds to the input power to the battery. The value of reference battery current $I^*_{bd}$ depends on the level of state of battery, which is proportional to the battery voltage, $V_{dc}$ [12]. The charging is continued till the battery bank is charged to 110% of nominal bus voltage i.e. 252 V. The magnitude of the $I^*_{bd}$ is evaluated as follows,

$$I^*_{bd}=0.65\times (252-V_{dc}) \quad (23)$$

The constant factor '0.65' is chosen so that the battery charging current remains within 10% of AH and in trickle mode under all circumstances. Highest value of $I^*_{bd}$ becomes 25 A when $V_{dc}$ reaches $V_{dcmin}$ i.e. 213.5 V.

## IV. RESULTS AND DISCUSSION

The Simulink model of micro-grid fed by REGS is developed in Matlab. The solar panels and wind turbine are modeled using their functions. Fig. 7 shows the performance of the system when the wind generator is taken in an out of the system. Fig. 8 shows the performance of the system when solar PV system is taken in and taken out of the system. Both the above scenarios also discuss the MPPT operation through RSC and solar converter. Fig. 9 shows results at loss of load and Fig. 10 at unbalanced nonlinear load. Fig. 11 shows a scenario when stored energy and generated power are low and external charging requirement through RSC is activated. Fig. 12 shows scenario when DC bus voltage is running at high charging power.

### *A. Performance of System at Constant Load and Cut-in and Cut-out of Wind Power*

As shown in Fig. 7, the system is started with 10 kW and 6 kVAR load without wind or solar energy sources. At t=2.25 s, the wind generator at wind speed of 7 m/s, is taken in service. As a result, a momentary fluctuation in the system voltage is observed. At t=6.0 s, the wind speed of turbine is increased from 7 m/s to 8 m/s followed by reduction of the wind speed to its original value at t=10.0 s. The rotor control action, maintains the desired rotational speed as per the W-MPPT algorithm. At t=14 s, the wind generator is taken out of service.

During cut-in and cutout of wind generator, momentary, the voltage surge is observed. The duration and magnitude of the voltage surge, are within an IEEE 1547 standard.

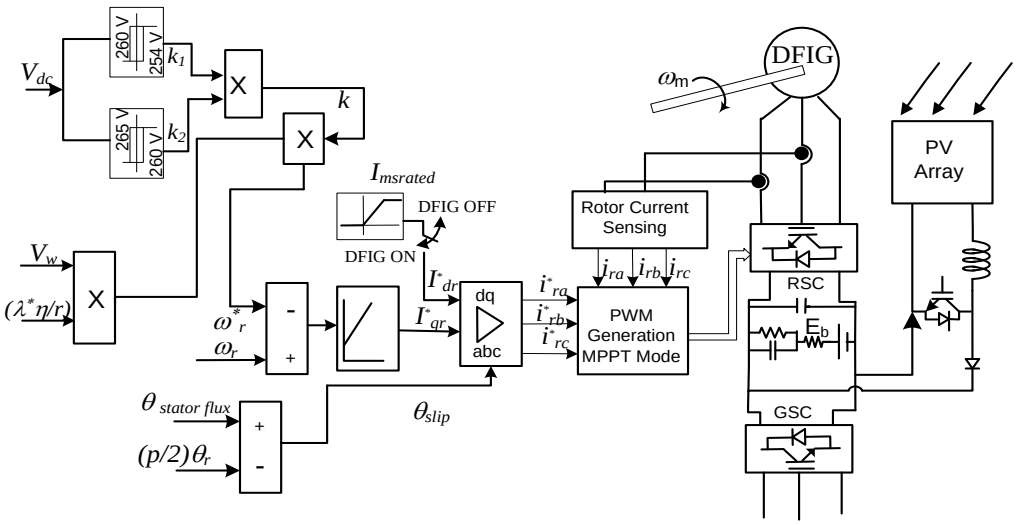


Fig. 5 Control diagram of RSC for REGS fed micro-grid

This article has been accepted for publication in a future issue of this journal, but has not been fully edited. Content may change prior to final publication. Citation information: DOI 10.1109/TIA.2018.2793213, IEEE Transactions on Industry Applications



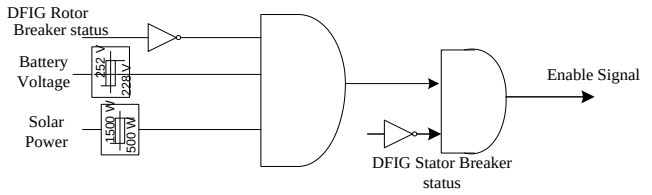


Fig. 6 Logic diagram for battery charging mode selection.

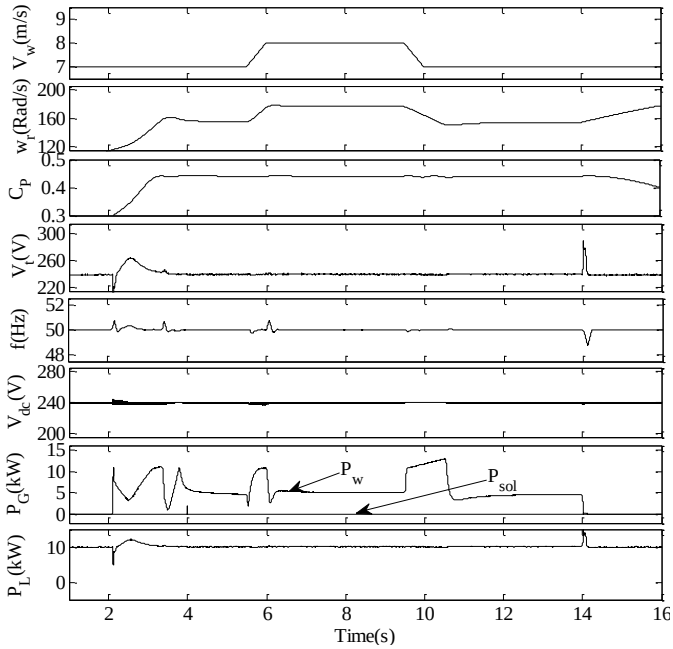


Fig. 7 Performance of REGS fed micro-grid with wind energy source

### *B. Performance of System at Constant Load and Cut-in and Cut-out of Solar Power*

The system is started with a 10 kW and 6 kVAR load without wind or solar energy. As shown in Fig. 8, at t=2.25 s, solar system is taken into the service at radiation of 800 W/m$^2$. At t=4 s, the solar radiation is raised to 900 W/m$^2$ and again it is reduced to 800 W/m$^2$ at t=6 s. The solar converter adjusts the solar PV voltage and operates at S-MPPT. At t=7 s, the solar system is taken out of service. No significant variation of system voltage is observed at any transition point.

### *C. Performance of System at Unbalanced Nonlinear Load*

The performance of the system at unbalanced nonlinear is shown in Fig. 9. A micro-grid should be suitable to provide requirement of unbalanced nonlinear load. A worst case scenario is taken when there are no generating sources. The connected load consists of 2 kW linear load and 8 kW nonlinear load. At t=3.25 s, the load of a-phase is disconnected from the network followed by b-phase load at t=3.46 s. It is seen from the results that the system is able to provide quality power to its customer in case of unbalanced as well as nonlinear load.

### *D. Performance of System at Loss of Load*

The performance of the micro-grid for loss of load, is shown in Fig. 10. A 10 kW and 6 kVAR load, is connected at the terminals prior to start of simulation. Neither wind nor solar power, is available and the load is fed by the battery. At t=2 s, the system load is disconnected. It is found that the system voltage and frequency remain constant of the network.

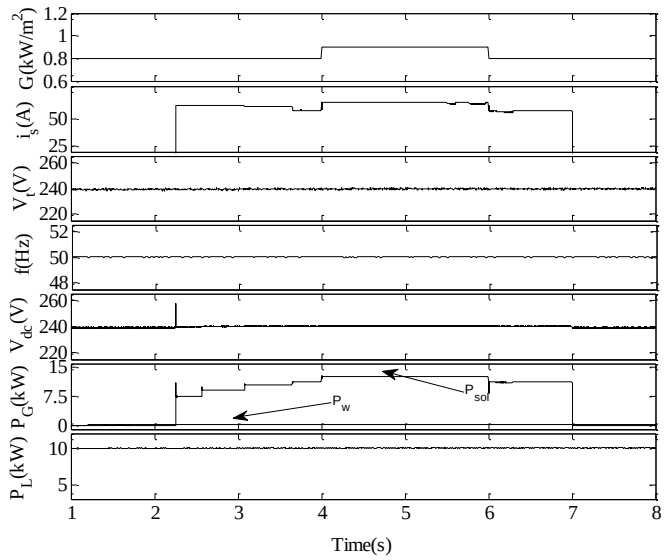


Fig. 8 Performance of the system without generating source and solar system is taken in the service.

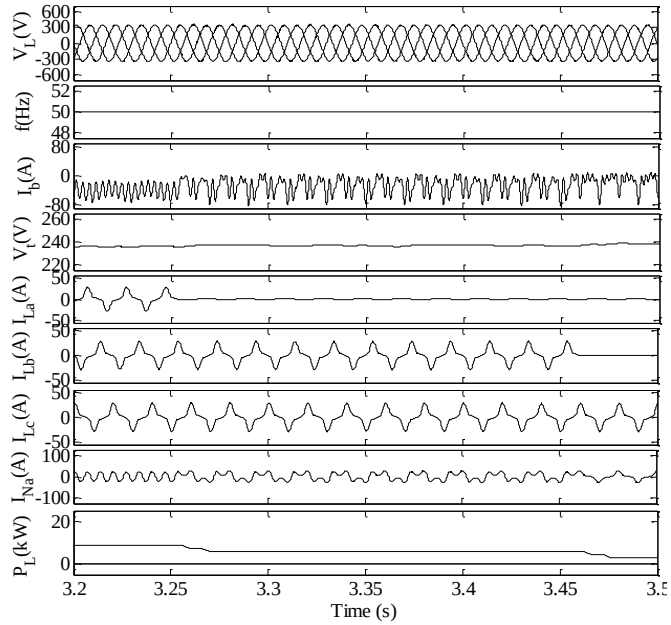


Fig. 9 Performance of the system at unbalanced and nonlinear load

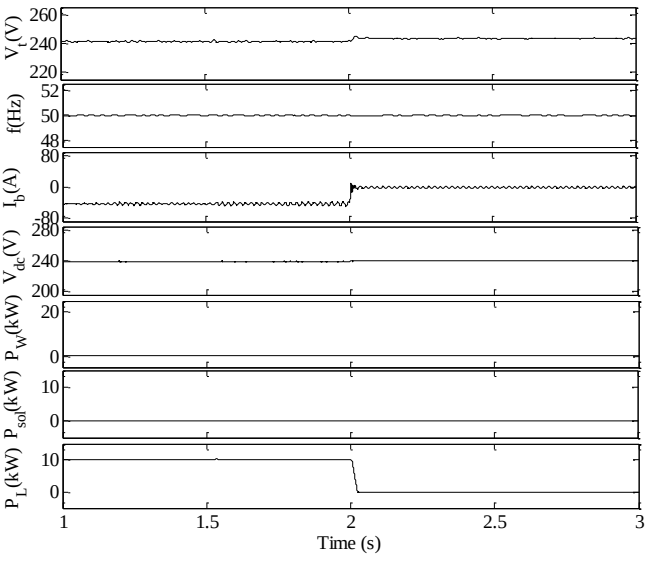


Fig.10 Performance of the system under loss of load at battery power

This article has been accepted for publication in a future issue of this journal, but has not been fully edited. Content may change prior to final publication. Citation information: DOI 10.1109/TIA.2018.2793213, IEEE Transactions on Industry Applications



### *E. System Running without Generating Source and Battery Charged from the Grid*

Fig. 11 shows the scenario when there are no generating sources feeding to the network combined with low battery. External charging is required to sustain the load requirement. Charging circuit is enabled as per the logic diagram of Fig. 6. At t=4 s, wind generation is taken out of service and because of lower battery voltage, the charging circuit is initiated. As a result external power is injected through the RSC to cater load requirement in addition to charging the batteries.

### *F. Performance of System during High Generation and Over-voltage Scenario of DC bus*

Performance of system at high net generation and over-voltage scenario of DC bus, is shown in Fig. 12. To make the effect visible, the AH of the battery is reduced by 1/200 times. The wind speed and solar irradiance, are kept 9 m/s and 700 W/m$^2$ respectively. It is seen from the curve, that once the $V_{dc}$ reaches 260 V, RSC control reduces the DFIG speed set point to 85% of the MPPT set point. It is seen from Fig. 12 that charging power, $P_c$ is reduced and the voltage rise is reduced.

## V. EXPERIMENTAL RESULTS

The proposed micro-grid system is realised in the laboratory using a 3.7 kW wound rotor induction machine as DFIG powered by a DC shunt motor. The solar energy system consists of a solar PV array simulator of a capacity 5 kW. The DC motor with intelligent torque control through buck converter, helps in achieving the wind turbine characteristics. The technical details of the wound rotor induction machine used as DFIG and DC motor used in these experiments, are given in Appendix-B and Appendix-C, respectively. Two numbers of 25 A IGBTs (Insulated Gate Bipolar Transistors) based VSCs (Semikron Make), are used as LSC and RSC. A set of 40 numbers of 12 V, 7 AH seal maintenance free batteries, are arranged in two parallel circuits to attain 240 V at the DC bus of VSCs. A digital controller (DS 1103 R&D) provides switching signals to all converters. The stator terminals of DFIG, are connected to the LSC through a zig-zag transformer. The generator speed is sensed using an encoder and the view of the complete experimental system is shown in Fig. 13. Fig 14(a) shows the experimental results for W-MPPT operation with the change in the wind speed. Fig. 14(b) shows S-MPPT with the change in the solar radiation. Fig. 15 shows the steady state values of electrical quantities and their harmonic spectra. Fig. 16 show test results when the micro-grid is without the wind power source and the load followed by the connection and disconnection of the load to the grid. Figs. 17 and 18 shows test results for the wind generator disconnection and the reconnection to the micro-grid, respectively. These test results demonstrate the satisfactory operation of the proposed micro-grid under different operating conditions.

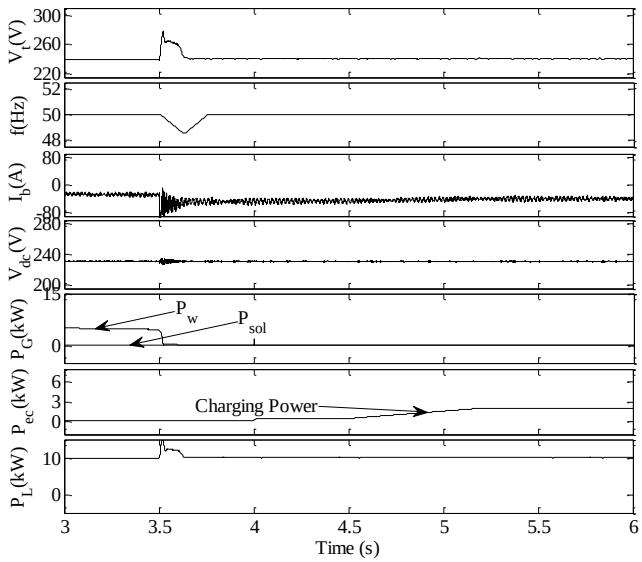


Fig. 11 Performance of system through external charging

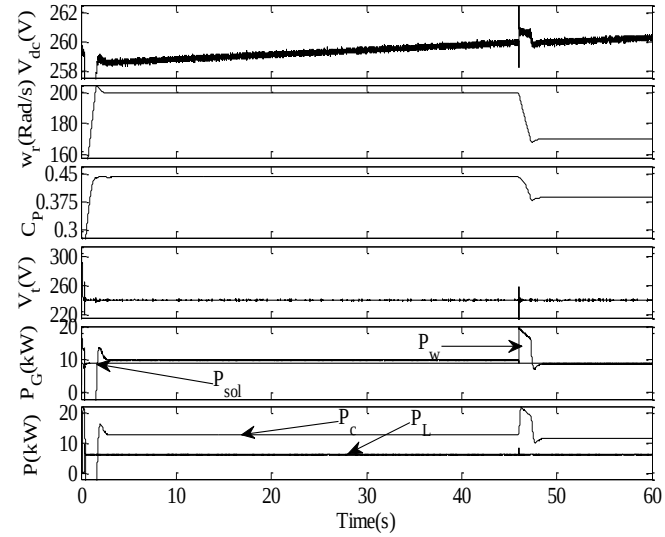


Fig. 12 Performance of system during high generation and over-voltage scenario of DC bus

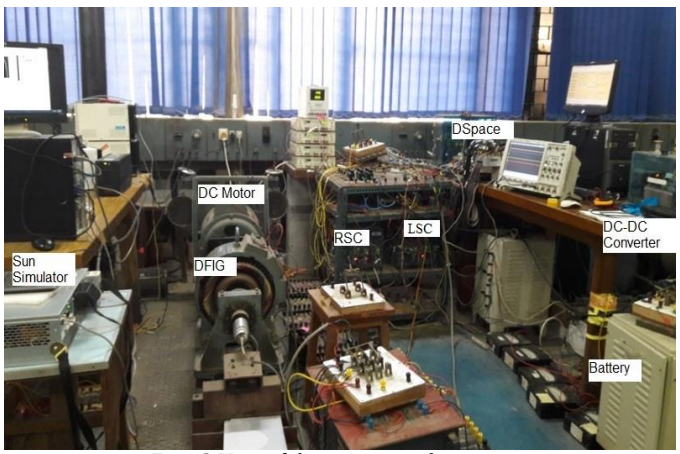


Fig. 13 View of the experimental prototype

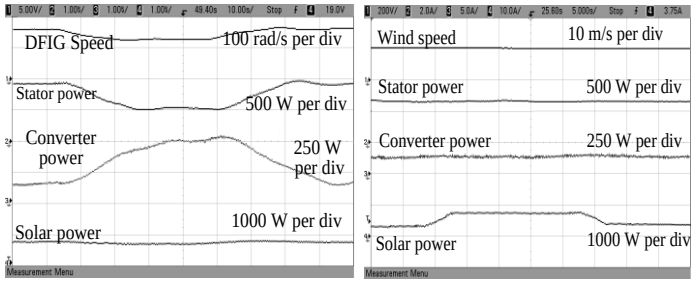


(a) (b)

Fig.14 Test result of REGS at (a) varying wind speed (b) varying solar radiation

This article has been accepted for publication in a future issue of this journal, but has not been fully edited. Content may change prior to final publication. Citation information: DOI 10.1109/TIA.2018.2793213, IEEE Transactions on Industry Applications



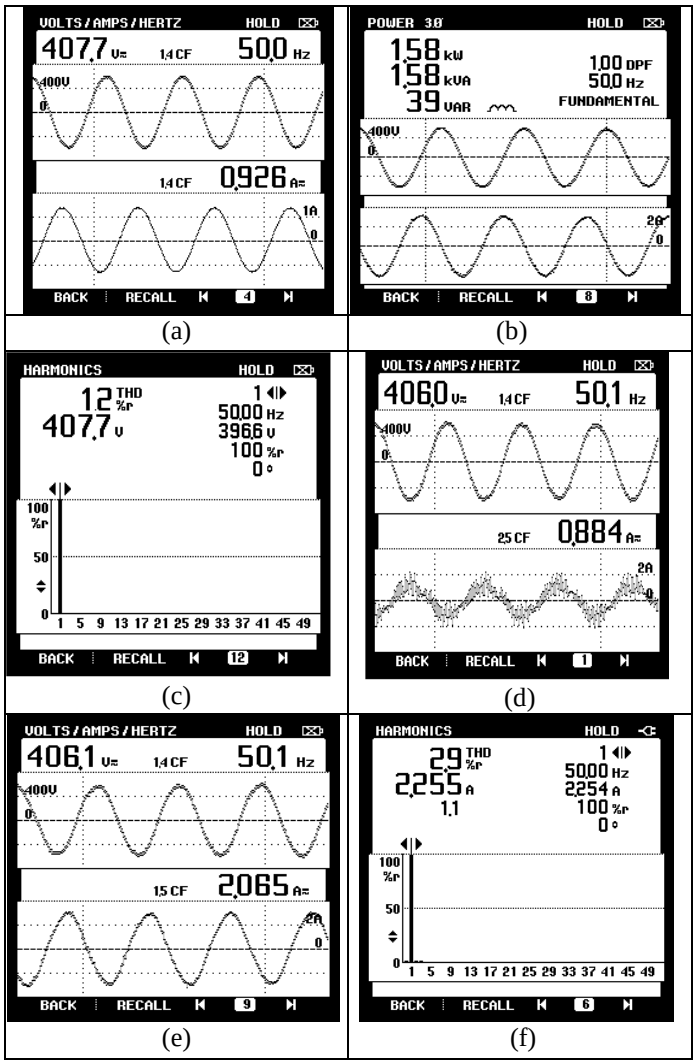


Fig.15 Test results at steady state (a) $i_{La}$ vs $v_{ab}$, (b) power at DFIG stator terminal, (c) Harmonic spectrum of $v_{ab}$, (d) LSC current, (e) $i_{sa}$ vs $v_{ab}$, (f) harmonic spectrum of $i_{sa}$

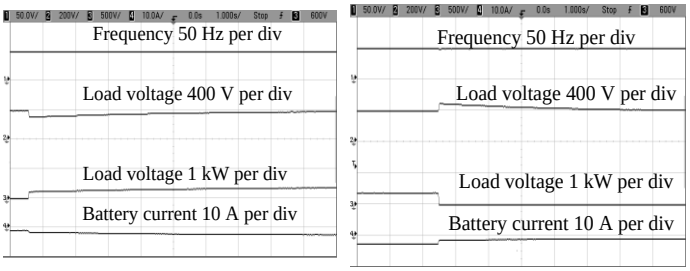


Fig.16 Test result for transient response of REGS without wind generator at (a) instant of cut-in of load (b) at removal of all load

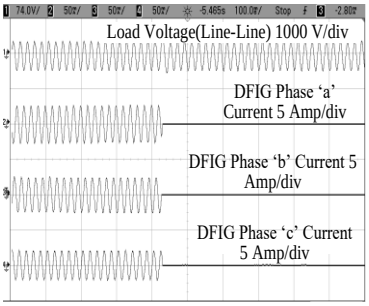


Fig. 17 Test result of line voltage and generator current of REGS during disconnection of wind generator

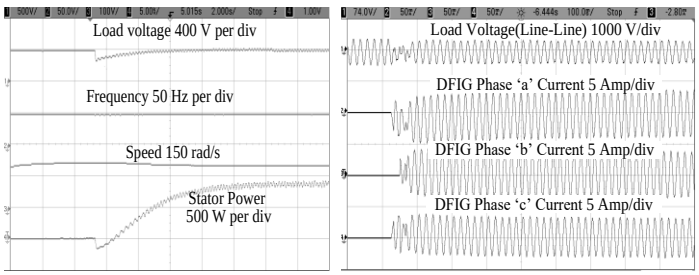


Fig. 18 Test Results during connection to micro grid, (a) Line r.m.s voltage, Frequency, speed and stator power, (b) Line voltage and currents

## VI. CONCLUTION

The proposed micro-grid system fed from REGS has been found suitable for meeting load requirement of a remote isolated location comprising few households. REGS comprises of wind and solar energy blocks, which are designed to extract the maximum power from the renewable energy sources and at the same time, it provides quality power to the consumers. The system has been designed for complete automated operation. This work also presents the sizing of the major components. The performance of the system has been presented for change in input conditions for different type of load profiles. Under all the conditions, the power quality at the load terminals, remains within acceptable limit. The effectiveness of the system is also presented with test results with prototype in the laboratory. The system has also envisaged the external battery charging by utilizing the rotor side converter and its sensors for achieving rectifier operation at unity power factor.

## APPENDICES

*A. Parameters of DFIG (Simulation)*

12.5 kW, 4 Pole, 415 V, 50 Hz, Y-connected, $R_s$=0.2692 Ω, $L_s$=81.62 mH, $R_r$=0.2701 Ω, $L_r$=83.43 mH, $L_m$=81.34 mH, Inertia=1 kg-$m^2$.

*B. Parameters of DFIG (Experimental)*

Make- McFEC Ltd, Capacity 3.7 kW, 400 V, 50 Hz, 4 Pole, Y-connected, $R_s$=1.32 Ω, $R_r$=1.708 Ω, $L_m$=219 mH, $L_{ls}$=6.832 mH, $L_{lr}$=6.832 mH, Inertia=0.1878 kg-$m^2$.

*C. Parameters of DC Machine (Prime Mover)*

Capacity 5 kW, 230 V, $R_a$=1.3 Ω, $R_f$=220 Ω, $L_a$=7.2 mH, $L_f$=7.5 H, Kφ=1.3314

*D. Controllers Gains*

PI gain of Speed controller: $K_{pr}$ = 12.5, $K_{ir}$ = 50
PI Voltage controller: $K_{pv}$ = 0.45, $K_{iv}$ = 2.5
Frequency controller $K_{p\omega e}$=0.1, $K_{i\omega e}$=0.01

## REFERENCES

[1] H. Zhu, D. Zhang, H. S. Athab, B. Wu and Y. Gu, "PV Isolated Three-Port Converter and Energy-Balancing Control Method for PV-Battery Power Supply Applications," *IEEE Transactions on Industrial Electronics*, vol. 62, no. 6, pp. 3595-3606, June 2015.

[2] M. Das and V. Agarwal, "Novel High-Performance Stand-Alone Solar PV System With High-Gain High-Efficiency DC–DC Converter Power Stages," *IEEE Transactions on Industry Applications*, vol. 51, no. 6, pp. 4718-4728, Nov.-Dec. 2015.

[3] A. B. Ataji, Y. Miura, T. Ise and H. Tanaka, "Direct Voltage Control With Slip Angle Estimation to Extend the Range of Supported Asymmetric Loads for Stand-Alone DFIG," *IEEE Transactions on Power Electronics*, vol. 31, no. 2, pp. 1015-1025, Feb. 2016.

[4] N.A. Orlando, M. Liserre, R.A. Mastromauro and A. Dell'Aquila, "A survey of control issues in PMSG-based small wind turbine system," *IEEE Trans. Industrial Informatics*, vol.9, no.3, pp 1211-1221, July 2013.

This article has been accepted for publication in a future issue of this journal, but has not been fully edited. Content may change prior to final publication. Citation information: DOI 10.1109/TIA.2018.2793213, IEEE Transactions on Industry Applications



[5] T. Hirose and H. Matsuo, "Standalone Hybrid Wind-Solar Power Generation System Applying Dump Power Control Without Dump Load," *IEEE Trans. Industrial Electronics*, vol. 59, no. 2, pp. 988-997, Feb. 2012.
[6] Z. Qi, "Coordinated Control for Independent Wind-Solar Hybrid Power System," *2012 Asia-Pacific Power and Energy Engineering Conference*, Shanghai, 2012, pp. 1-4.
[7] M. Rezkallah, S. Sharma, A. Chandra and B. Singh, "Implementation and control of small-scale hybrid standalone power generation system employing wind and solar energy," *2016 IEEE Industry Applications Society Annual Meeting*, Portland, OR, 2016, pp. 1-7.
[8] A. Hamadi, S. Rahmani, K. Addoweesh and K. Al-Haddad, "A modeling and control of DFIG wind and PV solar energy source generation feeding four wire isolated load," *IECON 2013 - 39th Annual Conference of the IEEE Industrial Electronics Society*, Vienna, 2013, pp. 7778-7783.
[9] S. K. Tiwari, B. Singh and P. K. Goel, "Design and control of autonomous wind-solar energy system with DFIG feeding 3-phase 4-wire network," *2015 Annual IEEE India Conference (INDICON)*, New Delhi, 2015, pp. 1-6.
[10] S. K. Tiwari, B. Singh and P. K. Goel, "Design and control of micro-grid fed by renewable energy generating sources," *2016 IEEE 6th Inter. Conference on Power Systems (ICPS)*, New Delhi, 2016, pp. 1-6.
[11] H. Polinder, F. F. A. van der Pijl, G. J. de Vilder and P. Tavner, "Comparison of direct-drive and geared generator concepts for wind turbines," *IEEE International Conference on Electric Machines and Drives, 2005.*, San Antonio, TX, 2005, pp. 543-550.
[12] Emmanouil A. Bakirtzis and Charis Demoulias "Control of a micro-grid supplied by renewable energy sources and storage batteries," XXth Inter. Conf. on Electrical Machines (ICEM), pp. 2053-2059, 2-5 Sept. 2012.
[13] S. Heier, Grid Integration of Wind Energy Conversion Systems. Hoboken,NJ: Wiley, 1998.
[14] Z.M. Salameh, M.A. Casacca and W.A. Lynch, "A mathematical model for lead-acid batteries," *IEEE Trans. Energy Convers.*, vol. 7, no. 1, pp. 93-97, Mar.1992.
[15] A B. Rey-Boué, R García-Valverde, F de A. Ruz-Vila and José M. Torrelo-Ponce, "An integrative approach to the design methodology for 3-phase power conditioners in Photovoltaic Grid-Connected systems," *Energy Conversion and Management*, vol. 56, pp. 80–95, Dec 2011.
[16] Z Xuesong,Song Daichun,Ma Youjie and Cheng Deshu, "The simulation and design for MPPT of PV system based on incremental conductance method," *2010 WASE Inter. Conf. on Information Engineering*, Aug, 2010, pp.314 –317.
[17] Shailendra. Kr. Tiwari, B. Singh and P. K. Goel, "Design and Control of Autonomous Wind-Solar Hybrid System with DFIG Feeding a 3-Phase 4-Wire System," in *IEEE Transactions on Industry Applications*, vol. PP, no. 99, pp. 1-1.

**Shailendra Kumar Tiwari (M'17)** received his B.E. (Electrical) from Govt. Engineering College, Raipur(Now NIT Raipur) India, in 1996. In 1997 he joined NTPC Ltd as Engineer, Power Plant Commissioining. In 2007, he did his M. Tech. (Power Generation Technology). from the IIT Delhi, through company sponsered programme. Presently, he is working as Additional General Manager in its Project Engineering Department, at Noida, Near New Delhi. His area of research is solar and wind energy conversion, solar energy estimation.

**Bhim Singh (SM'99, F'10)** was born in Rahamapur, Bijnor (UP), India, in 1956. He received his B.E. (Electrical) from University of Roorkee, India, in 1977 and his M. Tech. (Power Apparatus & Systems) and Ph.D. from the IIT Delhi, India, in 1979 and 1983, respectively. In 1983, he joined the Department of Electrical Engineering, University of Roorkee (Now IIT Roorkee), as a Lecturer. He became a Reader there in 1988. In December 1990, he joined the Department of Electrical Engineering, IIT Delhi, India, as an Assistant Professor, where he has become an Associate Professor in 1994 and a Professor in 1997. He has been ABB Chair Professor from September 2007 to September 2012. Since October 2012, he is CEA Chair Professor. He has been Head of the Department of Electrical Engineering at IIT Delhi from July 2014 to August 2016. Since, August 2016, he is the Dean, Academics at IIT Delhi. He is JC Bose Fellow of DST, Government of India since December 2015.

Prof. Singh has guided 69 Ph.D. dissertations, and 167 M.E./M.Tech./M.S.(R) theses. He has been filed 29 patents. He has executed more than eighty sponsored and consultancy projects. He has co-authored a text book on power quality: *Power Quality Problems and Mitigation Techniques* published by John Wiley & Sons Ltd. 2015.

His areas of interest include solar PV grid interface systems, microgrids, power quality monitoring and mitigation, solar PV water pumping systems, improved power quality AC-DC converters, power electronics, electrical machines, drives, FACTS, and high voltage direct current (HVDC) systems.

Prof. Singh is a Fellow of the Indian National Academy of Engineering (FNAE), The Indian National Science Academy (FNA), The National Academy of Science, India (FNASc), The Indian Academy of Sciences, India (FASc), The World Academy of Sciences (FTWAS), Institute of Electrical and Electronics Engineers (FIEEE), the Institute of Engineering and Technology (FIET), Institution of Engineers (India) (FIE), and Institution of Electronics and Telecommunication Engineers (FIETE) and a Life Member of the Indian Society for Technical Education (ISTE), System Society of India (SSI), and National Institution of Quality and Reliability (NIQR).

He has received Khosla Research Prize of University of Roorkee in the year 1991. He is recipient of JC Bose and Bimal K Bose awards of The Institution of Electronics and Telecommunication Engineers (IETE) for his contribution in the field of Power Electronics. He is also a recipient of Maharashtra State National Award of Indian Society for Technical Education (ISTE) in recognition of his outstanding research work in the area of Power Quality. He has received PES Delhi Chapter Outstanding Engineer Award for the year 2006. Professor Singh has received Khosla National Research Award of IIT Roorkee in the year 2013. He is a recipient of Shri Om Prakash Bhasin Award-2014 in the field of Engineering including Energy & Aerospace. Professor Singh has also received IEEE PES Nari Hingorani Custom Power Award-2017.

He has been the General Chair of 2006 IEEE International Conference on Power Electronics, Drives and Energy Systems (PEDES'2006), General Co-Chair of the 2010 IEEE International Conference on Power Electronics, Drives and Energy Systems (PEDES'2010), General Co-Chair of the 2015 IEEE International Conference (INDICON'2015), General Co-Chair of 2016 IEEE International Conference (ICPS'2016) held in New Delhi.

**Puneet Kr. Goel** was born in New Delhi, India, in 1966. He received his B.Tech in Electrical Engineering from IIT-Kanpur, India, in 1987; M.Tech. Degree in Power Apparatus & Systems from IIT-Delhi, India in 1989; M.S. in Electrical Engineering from U.S.C., Los Angeles, USA in 2001 and Ph.D. from IIT-Delhi, India in 2009. He joined Indian Administrative Services in 1991. His assignments include Secretary (Power), Andaman & Nicobar Islands, India; Director (Thermal), Ministry of Power, Govt. of India; Executive Director, Rural Electrification Corporation of India Limited; CMD, Delhi Transco and Secretary (Power), Govt. of NCT of Delhi. Currently, he is working as Commissioner, South Delhi Municipal Corporation, New Delhi, India.

His areas of research include Distributed and Stand Alone Power Generation using Renewable Sources of Energy